

Turbulence measurements in a three-dimensional boundary layer in supersonic flow

By WOLFGANG KONRAD† AND ALEXANDER J. SMITS

Department of Mechanical and Aerospace Engineering, Princeton University,
Princeton, NJ 08544-0710, USA

(Received 2 December 1996 and in revised form 10 November 1997)

Turbulence measurements were obtained in a three-dimensional supersonic turbulent boundary layer. A 20° curved fin was used to generate a three-dimensional compression of a boundary layer at Mach 3 in the absence of shock waves. Data include hot-wire measurements of five components of the Reynolds stress tensor. The results are interpreted in terms of the mean flow field history of the turbulence. It is demonstrated that in-plane curvature can have a strong stabilizing effect on the turbulence.

1. Introduction

Here, we describe the behaviour of a pressure-driven three-dimensional turbulent boundary layer generated by a curved fin (see figure 1). All measurements were taken in the region where there were no shock waves present. The static pressure, the static pressure gradients, and the curvature of streamlines increase gradually along the mean flow direction, so that the effects of increasing three-dimensionality can be examined in a single experiment. This is in contrast to the more commonly studied three-dimensional shock-wave/boundary-layer interactions where very sharp gradients can occur. The simple, well-defined geometry of the curved fin may help to give insight into the effects of streamline curvature, compression and three-dimensionality produced by more complex three-dimensional geometries.

‘Isentropic’ compressions such as that studied here may also hold some promise for improving the efficiency of supersonic inlet designs. Inlet geometries commonly use shock-generated compression which can result in large total pressure losses. Moreover, shock-generated interactions lead to a high degree of distortion of the mean flow, unsteady pressure loading due to shock movement, and strong secondary flows, all of which may be avoided or reduced by employing isentropic compressions generated by contoured walls.

Such flows have not been widely studied, in that only two similar studies have appeared in the literature. Hall (1965) reported extensive mean measurements in a Mach 1.6 S-shaped passage in which there was a reversal of direction of the crossflow, and Demetriades & McCullough (1985) generated a three-dimensional boundary layer using a curved twisted-wedge model in a Mach 3 flow. Hall found that the analyses by Mager (1952), Braun (1958), and Cooke (1958) for subsonic flows did not describe the flow well in regions of streamwise adverse pressure gradients, even after accounting for the variations in density. Johnston’s (1960) polar profiles also did not fit the data, and Hall attributed the discrepancy to the fact that the flow fields used in the respective investigations were not similar, a conclusion that was later confirmed by the analysis

† Present address: BMW AG, EA20, 80788 München, Germany.

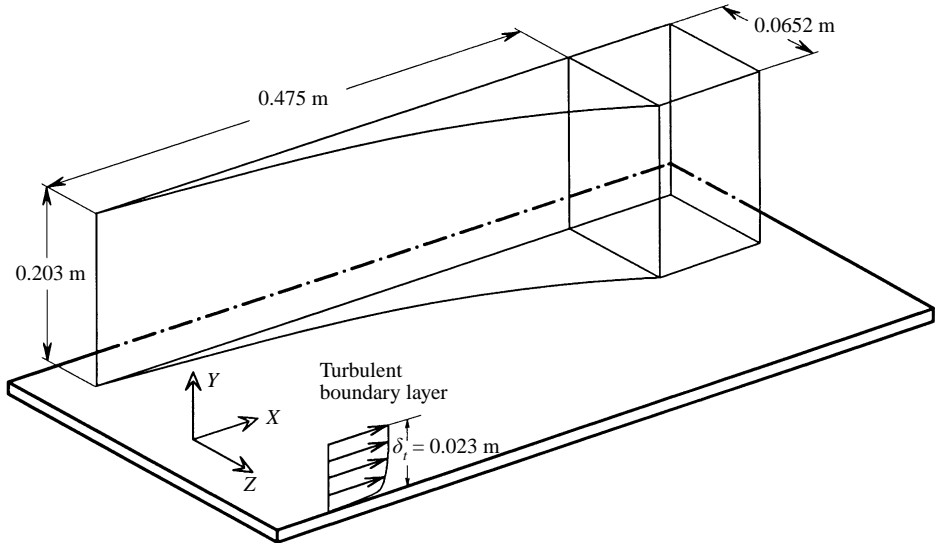


FIGURE 1. Curved-fin configuration (not to scale).

of Perry & Joubert (1965). The experimental model used by Demetriades & McCullough (1985) was designed to achieve zero streamwise pressure gradient while keeping the transverse pressure gradient constant. Only mean data were presented. The geometry was very different from that of Johnston's experiment, and it was therefore not surprising that the velocity profiles did not collapse according to Johnston's triangular plot. However, van den Berg's (1975) extended law of the wall was found to hold well up to $y^+ = 300$, probably because the crossflow angles were small ($< 6^\circ$ everywhere). Demetriades & McCullough also found a decrease in yaw angles in the viscous sublayer, a questionable result since a monotonic increase in yaw is expected as long as the pressure gradient does not decrease (see, for example, Degani 1991). The skin friction was measured using a Preston tube through the calibration suggested by Bradshaw & Unsworth (1974). The skin friction coefficients were not found to differ much from the corresponding two-dimensional flow, a result which can be attributed to the rather low level of three-dimensionality.

For supersonic flows with shock-induced three-dimensionality, a great deal more research has been performed, although very few turbulence data have been reported. Yanta, Ausherman & Hedlund (1982), and Ausherman & Yanta (1984), for example, tested a 7° semi-vertex-angle sharp cone for angles of attack of 0° , 2° , and 4° at a Mach number of 3. A laser Doppler velocimeter (LDV) was used to measure all three velocity components and the full Reynolds stress tensor. They found that the $\overline{u'^2}$ turbulence intensities were affected very little by roll angle or angle of attack, that is, with increasing three-dimensionality. The $\overline{v'^2}$ turbulence intensities were relatively constant across the boundary layer on the windward side and showed some increases with roll angle, while $\overline{w'^2}$ was insensitive to changes in either roll angle or angle of attack. The shear stress $-\overline{\rho u'v'}$ dropped slightly with increasing roll angle and angle of attack, which has also been found in subsonic studies of three-dimensional boundary layers (see, for example, Bradshaw & Pontikos 1985). The other two shear stresses were very small and only the $-\overline{\rho u'w'}$ stress exhibited increases near the wall when roll angle and angle of attack were increased.

Turbulence data were also obtained in a Mach 2.85 cylinder-flare flow by Kussoy *et al.* (1987) and Brown, Brown & Kussoy (1988). The three-dimensionality was

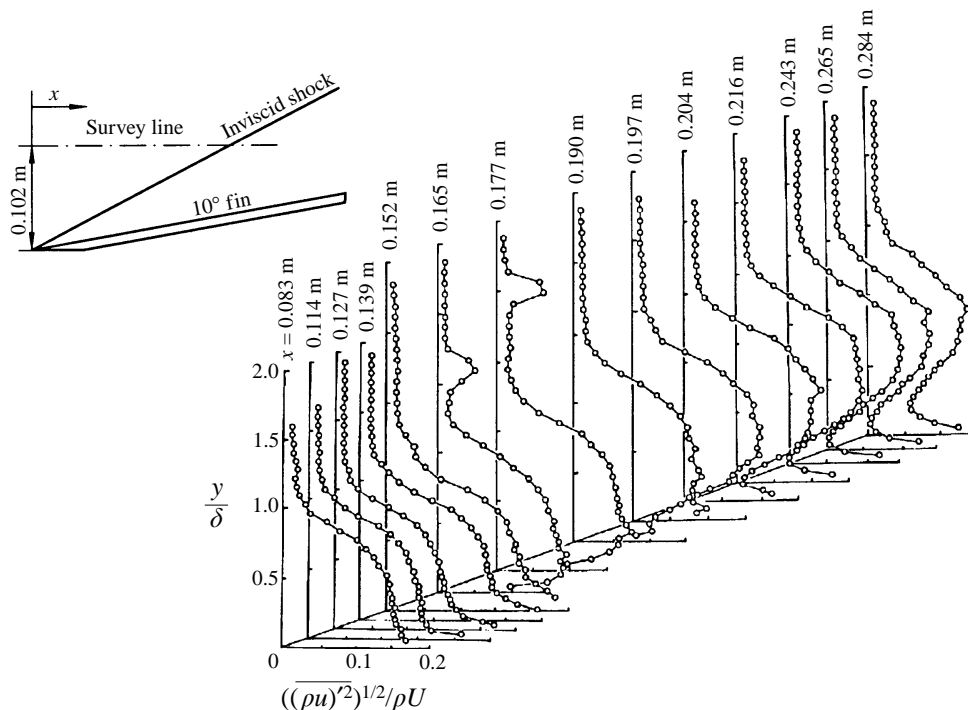


FIGURE 2. D. K. M. Tan's (unpublished) 10° sharp fin results.

generated by setting the cone at different angles of attack relative to the upstream cylinder. A strong shock was formed which separated the boundary layer. The LDV data include u' and v' measurements for two different angles of attack. As expected, higher angles of attack lead to stronger shocks and the turbulence kinetic energy was amplified accordingly.

A particular case of interest is the interaction generated by a 20° sharp fin at Mach 3. The sharp fin produces almost the same overall pressure rise as the curved fin used here, and the far fields of the two flows are very similar. This flow has been studied extensively by experiment and computation (see, for example, Settles & Teng 1983; Tran, Tan & Bogdonoff 1985; Knight *et al.* 1986; Shapey & Bogdonoff 1987; Alvi & Settles 1990; and Panaras 1992). However, the fluctuating wall pressure measurements by Tran *et al.* (1985) clearly display the unsteady nature of the sharp-fin interaction: for the 20° fin, the r.m.s. wall pressure fluctuations increased by a factor 7.2 through the interaction. No other turbulence data are available for the 20° fin case. A related experiment is the study of the 10° fin flow at Mach 2.9 by D. K. M. Tan (private communication). Tan used a hot wire to measure the component of the turbulence intensity in the direction of the local flow and found that in the downstream part of the interaction the turbulence levels first increased in the outer part of the boundary layer and then decreased in the lower half of the boundary layer (see figure 2).

It is difficult to understand the behaviour of turbulence in three-dimensional boundary layers in supersonic flows on the basis of these rather scattered data, taken in a number of widely different geometries. The flow studied here was designed to help to improve our understanding by avoiding the complexities introduced by shock waves, and by increasing the extent and degree of the three-dimensionality gradually through the interaction. The experimental work was strongly coupled to computations,

and the comparisons between experiment and computation on the structure of the mean flow field was reported by Konrad, Smits & Knight (1994, 1998). The primary focus of the present contribution is the turbulence behaviour. Except for $\overline{\rho v'w'}$, all components of the Reynolds stress tensor were measured using hot-wire anemometry. Large changes were found, indicating a highly non-isotropic response to the three-dimensionality. The results along a particular streamline (where the streamline was found from the computations) were also compared with results from a two-dimensional boundary layer with similar initial conditions and a matched pressure gradient (Fernando & Smits 1990), and the stabilizing effects of in-plane curvature were identified.

2. Experimental details and mean flow results

All experiments were performed in the high-Reynolds-number supersonic $0.203 \text{ m} \times 0.203 \text{ m}$ blowdown wind tunnel at the Princeton Gas Dynamics Laboratory. The upstream free-stream Mach number was $2.87 (\pm 1\%)$, with a total pressure of $6.89 \times 10^5 \text{ N m}^{-2} (\pm 1\%)$, and a nominal total temperature of approximately $265 \text{ K} (\pm 2\%)$. Wall conditions were nearly adiabatic ($T_w/T_{0_\infty} \approx 1.04$).

The boundary layer upstream of the fin developed on the floor of the wind tunnel, and transition developed naturally in the nozzle section. Downstream of the nozzle, the boundary layer developed in a nominally zero pressure gradient. The characteristics of this boundary layer have been extensively documented (see Settles 1975; Smits & Muck 1984) and the data demonstrate that the boundary layer is fully developed and self-preserving. Some minor spanwise non-uniformity was found, probably due to the inlet to the tunnel nozzle and the growth of the sidewall boundary layers. The divergence from two-dimensionality is relatively small (less than $\pm 5\%$ in the skin friction coefficient C_f over $5\delta_\infty$, where δ_∞ is the incoming boundary layer thickness) and this was not expected to influence the results of the current investigation significantly. The incoming boundary layer parameters at $X = 0$, $Z = 0$ are as follows: $\delta_\infty = 25 \text{ mm} \pm 5\%$, $\delta^* = 6.1 \text{ mm} \pm 2\%$, $\theta = 1.1 \text{ mm} \pm 3\%$, $Re_\theta = 84000 \pm 5\%$, and $C_f = 0.00104 \pm 5\%$. All quantities are normalized by free-stream values.

The experimental configuration is shown in figure 1. A Cartesian coordinate system was used so that the origin was located on the centreline of the tunnel, 76.2 mm across from the leading edge of the fin. The fin was designed using the method of characteristics so that the inviscid focal point of the compression wave system was located 0.229 m spanwise from the leading edge, well outside the tunnel test section. The predicted streamwise location of the focal point was at $X = 0.615 \text{ m}$. The curved fin coordinates, where $(x, \Delta z)$ are the streamwise and spanwise locations, measured from the fin leading edge, are available from the authors or Konrad (1993).

The radius of curvature of the fin continually increased along its length, the length of the fin was 0.475 m , and the final fin angle was 20° , at which point an expansion corner was used to turn the flow in the direction of the tunnel axis. A sidewall boundary layer bleed was used on the wall opposite the fin to minimize the region where the compression waves interacted with the sidewall boundary layer.

The mean flow results were reported by Konrad *et al.* (1994, 1998) as part of the comparison with computations, and only a brief summary will be given here. Essentially, the good agreement found between experiment and computation, performed with a simple Baldwin–Lomax model, indicated that the flow studied here is rotational and inviscid, i.e. the turbulence model was not severely tested. A line of convergence appeared in the surface flow visualization that conveniently divides the

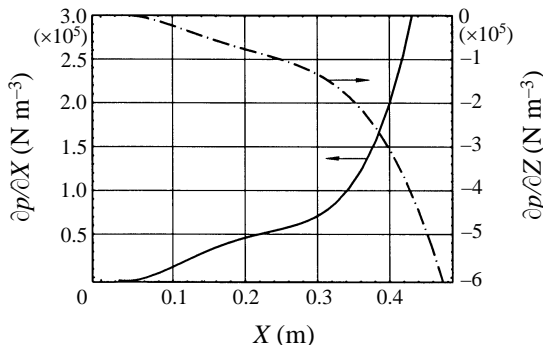


FIGURE 3. Streamwise and spanwise pressure gradient distributions along the line $Z = 0$.

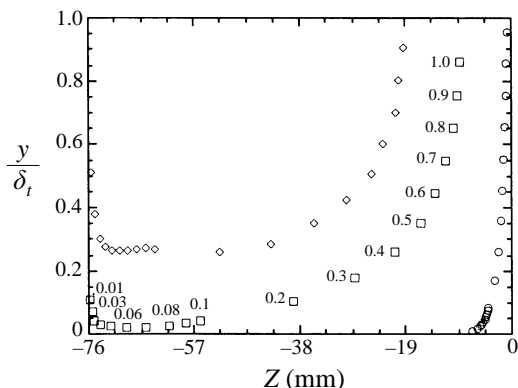


FIGURE 4. Initial ($X = 0$) heights of streamlines crossing the $Z = 0$ plane at: \circ , $X = 0.222$ m; \square , $X = 0.349$ m; \diamond , $X = 0.413$ m. Numbers indicate the value of y/δ_t at $X = 0$.

flow field into two regions. The upstream region can be further subdivided in two subdomains (the ‘small-crossflow region’ and the ‘upstream convergence region’), where 10° was taken as the maximum ‘small’ crossflow angle. On the centreline ($Z = 0$), the small-crossflow region extends to about $X = 0.25$ m, the upstream convergence region is bound downstream by the line of convergence (located at $X = 0.36$ m), and the downstream convergence region comprises the region downstream of the line of convergence.

The upstream convergence region includes crossflow of the order of 20° and increasing near-wall retardation, as typically found in adverse-pressure-gradient flows. In this region, pitch angles were very small, so that the streamline curvature was virtually confined to horizontal planes (‘in-plane’ curvature).

The strongest effects of three-dimensionality were seen in the downstream convergence region. While the velocity decreased in the outer part of the boundary layer, the near-wall part was greatly accelerated, although the pressure gradients in the X - and Z -directions continue to increase monotonically with streamwise distance (figure 3). Figure 4 indicates that this is due to the history of the mean flow development, that is, lower parts of the downstream boundary layer draw higher-momentum fluid from the incoming two-dimensional boundary layer. Stations further downstream on the centreline draw fluid from greater heights in the incoming layer; therefore they display even larger gradients near the wall. Figure 4 does not suggest that fluid is drawn from the boundary layer on the fin, as this boundary layer has zero

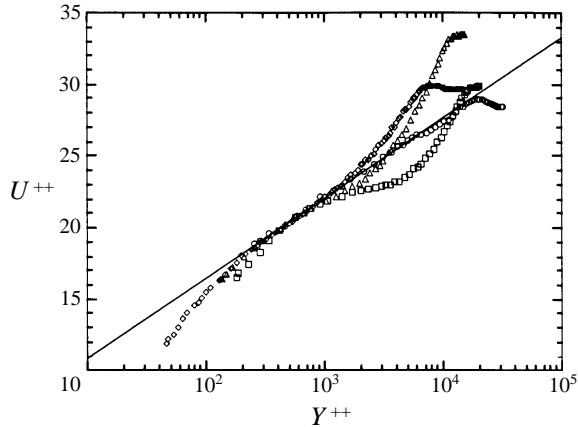


FIGURE 5. Van Driest (1951) transformed velocity profiles in inner coordinates along the line $Z = 0$: \diamond , $X = 0$; \triangle , $X = 0.349$ m; \square , $X = 0.413$ m; \circ , $X = 0.470$ m.

thickness at the leading edge of the fin. The maximum spanwise velocity component is reached at $X = 0.432$ m before the relaxation of the boundary layer leads to a decrease further downstream. Only the data in the upstream part of the flow field, where crossflow angles were small ($< 10^\circ$), were found to follow the Johnston (1960) triangular scaling. Figure 3 shows the spanwise and streamwise pressure gradients along the centreline and it is clear that both the wall pressures and the pressure gradients increase continuously in the streamwise and spanwise directions. Consistent with boundary layer theory, the static pressure remains approximately constant across the layer. Surprisingly, the local boundary layer thickness remained nearly constant throughout the flow field.

The magnitude of the velocity vectors in the local flow direction, transformed according to van Driest (1951) display a logarithmic region, even in the strongly three-dimensional flow field far into the interaction (see figure 5). At $X = 0.349$ m, a slight dip below the standard log law is seen to occur, which develops to its maximum extent at $X = 0.413$ m. Such dips are typically associated with two-dimensional flows experiencing concave streamline curvature (Spina, Smits & Robinson 1994), but in this case they most likely indicate the different history effects experienced by the inner and outer parts of the boundary layer, as described earlier. Further downstream, the boundary layer shows some sign of recovering, and at $X = 0.470$ m the dip in the outer part of the boundary layer has practically disappeared.

The skin friction coefficients were found using the Clauser (1956) chart and the Preston tube method (see figure 6). For supersonic two-dimensional turbulent boundary layers, these methods are extensively documented and they agree to within $\pm 10\%$, even in strongly perturbed flows (Smith *et al.* 1992), as long as the velocity profiles display a logarithmic region. The Preston tube method also appears to work well in strongly three-dimensional flows. It is relatively insensitive to changes in flow angle (Konrad 1993), and Kim, Lee & Settles (1991) showed encouraging agreement between Preston tube data and results derived from laser interferometry in a three-dimensional shock-wave boundary-layer interaction generated by a 10° sharp fin at Mach 3. In the present case, there is about a 10% to 20% difference between the results obtained by the two methods, and the difference remains approximately constant throughout the flow field. Since the error in the experimental data is estimated to be about $\pm 10\%$, the agreement found in figure 6 is rather satisfactory, although the

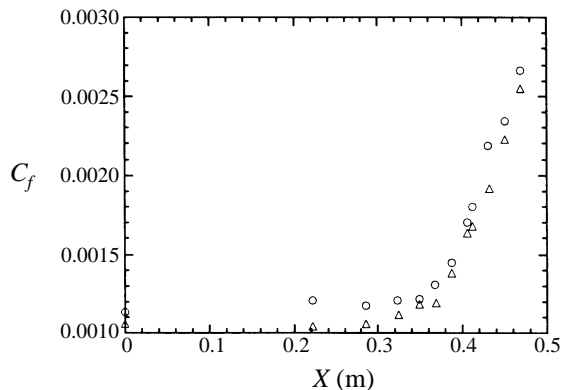


FIGURE 6. Skin friction distributions along the line $Z = 0$. ○, Clouser chart method on van Driest transformed velocity profiles; △, Preston tube results using Bradshaw & Unsworth's (1974) calibration with corrections by Allen (1977).

absolute accuracy of the data is still in question. A steep rise in the skin friction is seen at about $X = 0.36$ m, which corresponds to the location of the line of convergence detected in the surface flow visualization.

3. Hot-wire anemometry techniques

For the turbulence measurements, special probes and techniques needed to be developed. For example, it was particularly important to align the hot wires with the local flow direction to avoid interference due to shock waves emanating from the needle tips. The probes were therefore mounted in a rotatable plug, and the probe was aligned with the flow direction previously determined from a 3-hole Pitot probe survey to within $\pm 0.1^\circ$. Also, different probe shapes were tested using schlieren photography to determine the extent of the aerodynamic interference caused by the probe support geometry. In the final design, the vertical part of the probe support was shaped like a wedge so that the shock wave would remain attached for most of the vertical extent of the probe, and all probe dimensions were minimized. Surveys of the incoming two-dimensional boundary layer where the turbulence behaviour is well-documented (Fernando & Smits 1990) were also used to check the performance of the probe (see Konrad & Smits 1993 for further details). Finally, a 30° angle of inclination for the crossed-wires was chosen to reduce transonic effects and to decrease possible 'cone angle problems' (Perry *et al.* 1983 and Smits & Muck 1984).

The probes were connected to DANTEC DISA 55M12 symmetrical (1:1) bridge constant-temperature anemometers using external matching resistors. The frequency response for all wires was typically above 160 to 170 kHz. The frequency response was always set under conditions corresponding to the maximum mass flux encountered in the experiment. Kistler (1959) noted that to obtain the turbulence intensity to better than 5% accuracy, the frequency response for a normal hot wire should exceed $5U_\infty/\delta_\infty$ Hz, which corresponds to about 100 kHz in the present study. For crossed-wires, the criterion is more stringent, and Gaviglio, Anguillet & Elena (1981) implied that with the frequency response achieved here, $-\overline{\rho u'v'}$ may be underestimated by more than 10%. Additional errors may be introduced by wires with a mismatched frequency response since the phase differences can become very important in determining the shear stress. The frequency response of both wires was therefore matched as closely as possible.

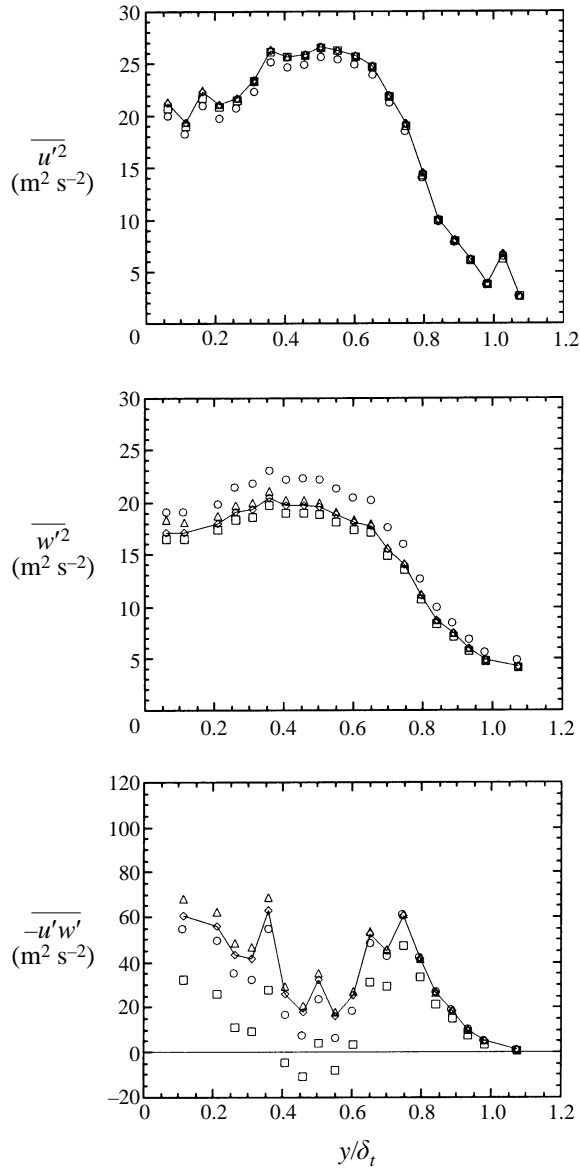


FIGURE 7. Comparison of uw -probe data for different trial corrections: \diamond , no correction; \square , probe misalignment; \triangle , wire misalignment; \circ , recalibration.

The wires were calibrated in the free stream of a small pilot facility by varying the mean mass flux ρU by changing the stagnation pressure. Correlations were made to account for the varying total temperature, as proposed by Smits, Hayakawa & Muck (1983). The output voltage E was fitted by least squares to determine the coefficients L and M in the following form of King's law:

$$E^2 = L + M(\rho u)^n$$

with $n = 0.55$. Under the flow conditions encountered in this experiment, the sensitivity of a hot wire in supersonic flow is virtually independent of Mach number except in the transonic regime where the exponent n demonstrates a strong Mach-number

Normal wire	$\overline{(\rho u)'^2}^{1/2}/\overline{\rho u}$	−5% to +9%
	$\overline{u'^2}^{1/2}/U$	−25% to −7%
Crossed-wire	$\overline{(\rho u)'^2}^{1/2}/\overline{\rho u}$	−7.5% to +7.5%
	$\overline{v'^2}^{1/2}/U$ and $\overline{w'^2}^{1/2}/U$	−15% to +7%
	$-\overline{\rho(\rho u)'v'}/\overline{\rho u^2}$ and $-\overline{\rho(\rho u)'w'}/\overline{\rho u^2}$	−27% to +11%
	$\overline{u'^2}^{1/2}/U$	−27% to −9%
	$-\overline{u'}/U^2$ and $-\overline{u'w'}/U^2$	−14% to +24%

TABLE 1. Hot-wire uncertainties

dependence. For normal wires, errors in the least-squares fit of E^2 were always less than 1%. For crossed-wires, the calibration followed the same general procedure but the response was written as

$$E_i^2 = L_i + M_i G_i(\phi) (\rho u)^n$$

where $G_i(\phi) = 1.0$, and $n = 0.55$ (see Smits & Muck 1984). The anemometer output is again virtually independent of the Mach number, except when the Mach number normal to the wire is in the transonic range. To calibrate $G_i(\phi)$, the function that determines the angular sensitivity, the mass flux was held constant and the yaw angle of the probe was varied continuously between $\pm 7^\circ$. The yaw sensitivity was found using the second-order Taylor method of Donovan & Spina (1992), rather than Smits & Muck's (1984) first-order Taylor method, since it was considered to be more accurate. The least-squares error in the yaw calibration was usually about 1% for the uw -probe and never exceeded 2% for the uw -probe. The King's law calibrations were of the same quality, and the least-squares errors were always less than 1%.

During data acquisition, the anemometer outputs were split and passed through 10 Hz low-pass and 10 Hz–400 kHz band-pass filters. The fluctuating signals were amplified and digitized at 1 MHz. The mean signal was halved in amplitude and digitized at 100 Hz. For normal wire runs, 96 K consecutive points of the fluctuating data were recorded, while for crossed-wires half that number of points for each channel was found sufficient to give satisfactory resolution of spectra and probability density functions. About 22–25 equally spaced points were taken for each boundary layer profile.

The wires were subsequently recalibrated to check for drift in the calibration coefficients. Unfortunately, the wires often broke at the end of the run or upon tunnel shutdown. Recalibration was only possible for about one third of the crossed-wire runs but for almost all the normal wire runs. However, many runs gave overlapping data which helped establish confidence in the repeatability of the measurements. In figure 7, data reduced with a set of recalibrated coefficients are compared to data obtained from the original calibration. Given the difficulties in making these measurements, this level of agreement was considered acceptable.

The uncertainty estimates for the turbulence data are given in table 1, and they are about twice those found in subsonic studies. The accuracies listed in table 1 are comparable to those produced with LDV systems in supersonic flows, e.g. Johnson & Rose (1975) and Deleuze & Eléna (1995) who performed measurements in zero-pressure-gradient boundary layers at Mach numbers of 2.9 and 2.3, respectively. A comparison of the data acquired with the uw -crossed-wire probe upstream of the interaction with Fernando & Smits' (1990) results in the same boundary layer is shown

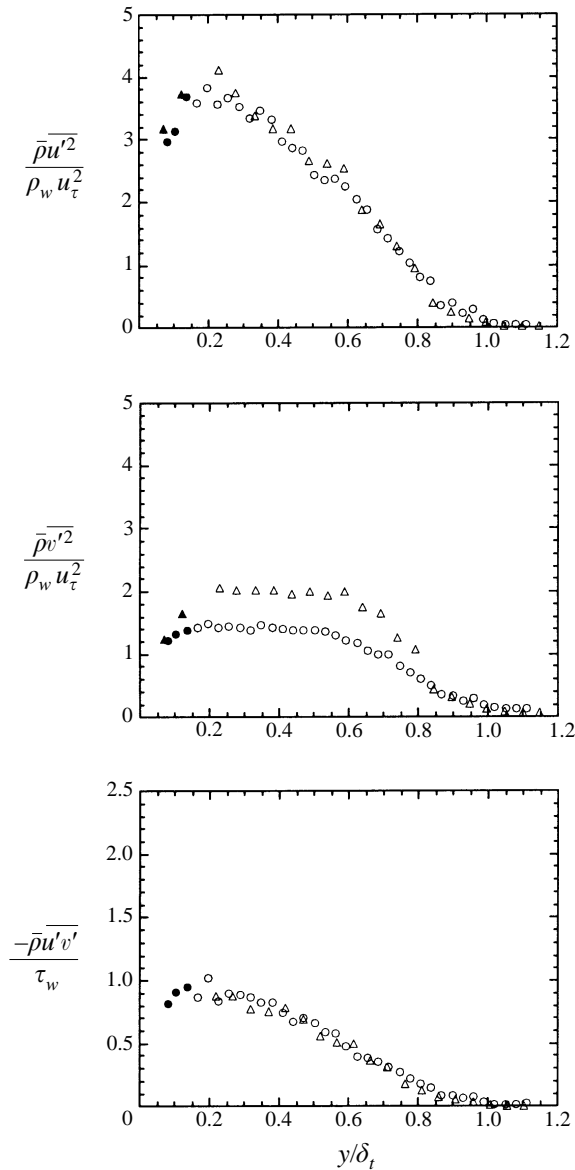


FIGURE 8. Turbulence levels in the upstream boundary layer: \triangle , present results; \circ , Fernando & Smits (1990). Filled-in symbols indicate that low-Mach-number effects were important and these results should be treated with caution.

in figure 8. Good agreement was found for $\overline{\rho u'^2}$ and the Reynolds shear stress $-\overline{\rho u'v'}$, but the agreement for $\overline{\rho v'^2}$ was not so satisfactory, although it is within the expected experimental error. It is possible that the discrepancies are due to the slightly different technique used by Fernando & Smits to find the yaw sensitivity of the crossed-wire probe. Note that in figure 8 and elsewhere the boundary layer thickness δ_t is the point where the Reynolds shear stress falls to 5% of its maximum value. This length scale seems more appropriate than the mean flow thickness in these highly distorted flows, as first suggested by Bradshaw (1973).

As indicated earlier, measurements of $\overline{w'^2}$ and $\overline{u'w'}$ in supersonic flows are very

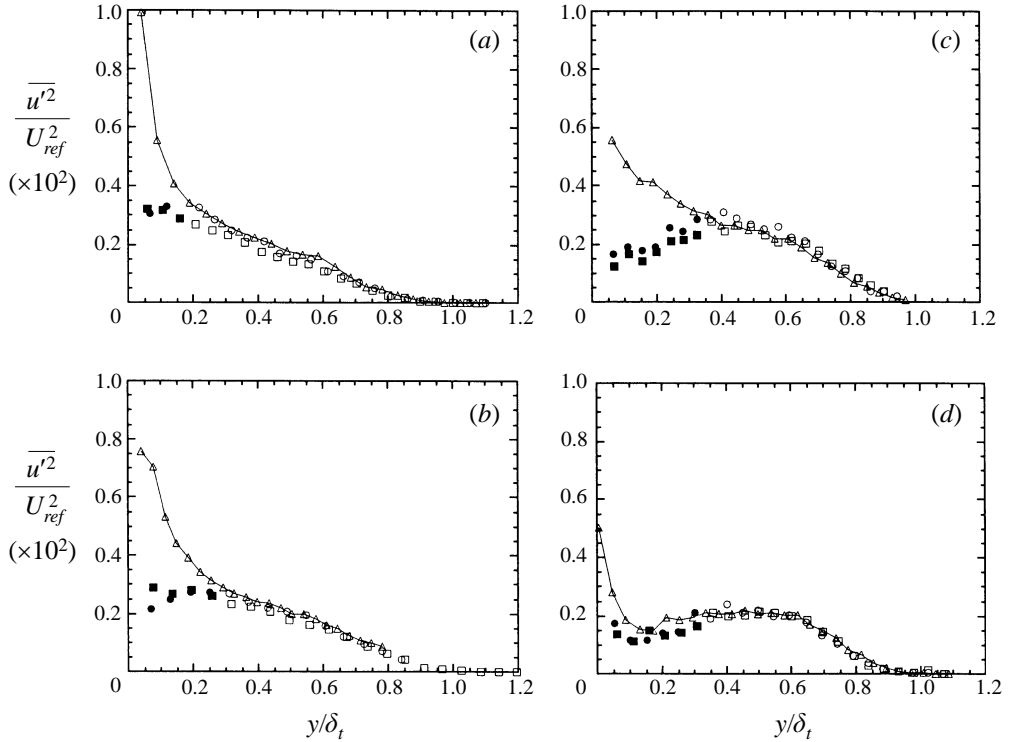


FIGURE 9. Streamwise turbulence levels measured by different probes: (a) $X = 0$ m; (b) $X = 0.222$ m; (c) $X = 0.349$ m; (d) $X = 0.413$ m. \triangle , Normal wire; \circ , uw -wire; \square , uw -wire. Filled-in symbols indicate that low-Mach-number effects were important and these results should be treated with caution.

scarce, and only one previous measurement of $\overline{u'w'}$ has been reported, by Ausherman & Yanta (1984), who used LDV. It is therefore not possible to assess the accuracy of these data by comparison with previous work. One way to assess the accuracy of the data presented here is to compare the streamwise turbulence intensities obtained using the uw -probe to those measured by the uw -crossed-wire and the normal-wire probes. This is shown in figure 9. The drop-off near the wall may be due to the different spatial resolutions of the probes, or to low-Mach-number effects, and filled-in symbols are used for the data near the wall to indicate that the uncertainties in this region exceed the levels given in table 1. The spatial resolution of the normal wire is set by its length, which is about 0.8–0.9 mm ($l/\delta_\infty = 0.034$), whereas the spatial resolution of the crossed-wire probes is set by the separation between the two wires, which was about 1.6 mm. However, the fact that the normal-wire and crossed-wire results for $\overline{u'^2}$ agree well throughout most of the layer suggests that low-Mach-number effects, rather than spatial resolution are the major problem. The drop-off appears to start at normal Mach numbers less than 1.5, which is a little earlier than the point where Smits *et al.* (1983) indicated that transonic effects become important. In principle, the spanwise Reynolds shear stress $-\overline{\rho u'w'}$ should be zero in the incoming two-dimensional boundary layer but it is not surprising that the measurements show levels up to 20% of the local wall shear stress. This may indicate a low level of three-dimensionality in the increasing boundary layer: the flow quality in a supersonic testing facility can be expected to be less than that of a good subsonic facility, but it may also reflect the level of the experimental uncertainty.

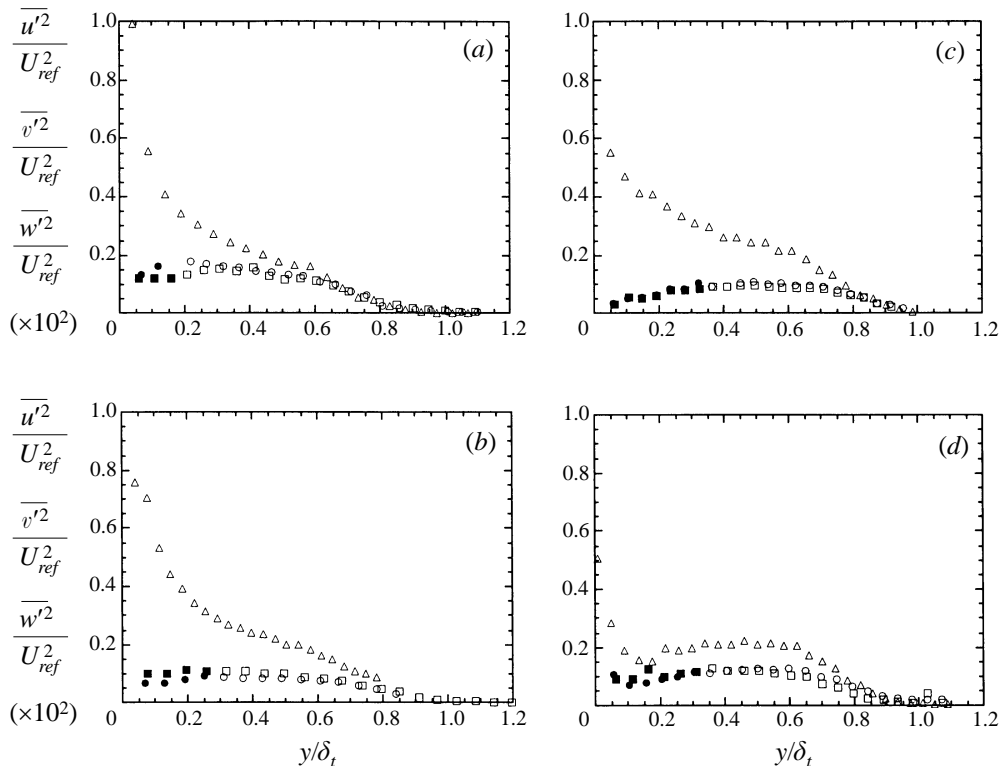


FIGURE 10. Kinematic turbulence levels: (a) $X = 0.000$ m; (b) $X = 0.222$ m; (c) $X = 0.349$ m; (d) $X = 0.413$ m. \triangle , $\overline{u'^2}/U_{ref}^2$; \circ , $\overline{v'^2}/U_{ref}^2$; \square , $\overline{w'^2}/U_{ref}^2$. Filled-in symbols indicate that low-Mach number effects were important and these results should be treated with caution.

Angular misalignment of the normal hot wire during calibration or data acquisition was estimated to about 1° . According to Smits & Muck (1984), the angular response of a probe in supersonic flow follows a cosine-square law, and a 1° misalignment will result in less than 1% error in measured turbulence intensity. For the uw -probe, angular misalignment stems mainly from the difficulty of matching the orientations of the probe during calibrations in the pilot tunnel and during data acquisition in the actual test facility. In addition, because the wires are separated by a vertical distance, the yaw angles are different for the two wires during measurement (the uw -probe was aligned with the mean flow direction corresponding to the average vertical wire position). The geometrical misalignment of the crossed-wire probes was checked by plotting the difference of the mean output voltages versus their sum. As Abell (1974) showed, this procedure provides an immediate check of the angular alignment (further details are given by Konrad 1993).

To assess the effects of the two different kinds of misalignments, some trial corrections were made using data taken for the uw -crossed-wire run at $X = 0.413$ m. Corrections were made by shifting the yaw calibration by 3° for the probe misalignment and similarly by correcting each wire separately for the flow direction, that is, the wire closer to the wall for a negative misalignment and the upper wire for a positive misalignment. In figure 7 it can be seen that the effect of the probe misalignment is significant, especially for the Reynolds shear stress, but that the effect of separate correction in the wire misalignment is almost negligible since the correction is approximately the same for the two wires, but of opposite sign. To put this into

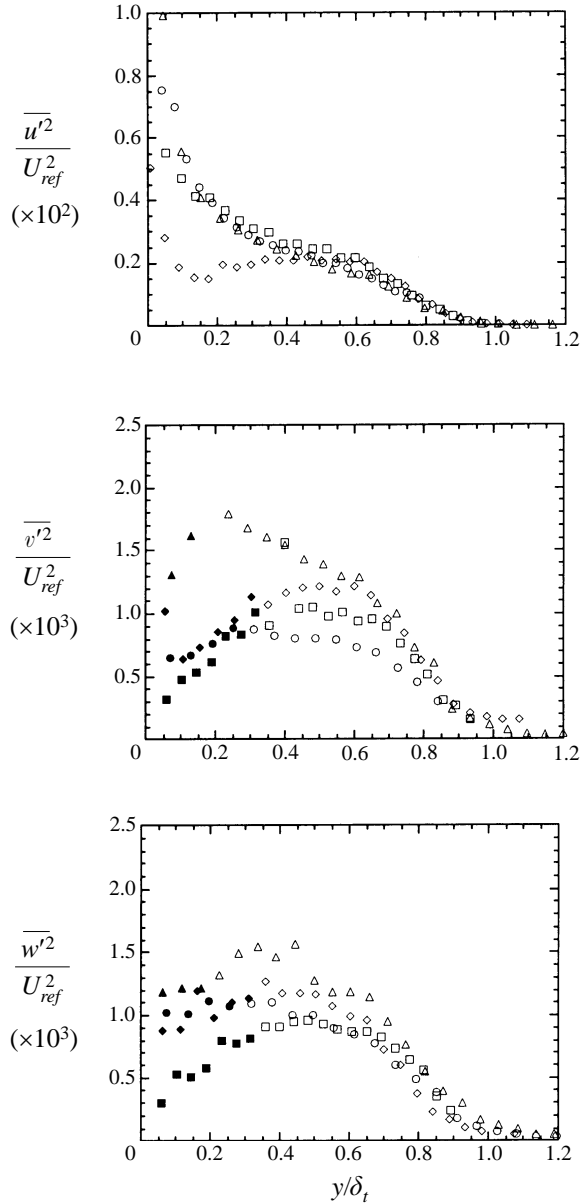


FIGURE 11. Kinematic turbulence levels normalized by the reference free-stream velocity: \triangle , $X = 0$ m; \circ , $X = 0.222$ m; \square , $X = 0.349$ m; \diamond , $X = 0.413$ m. Filled-in symbols indicate that low Mach number effects were important and these results should be treated with caution.

perspective, figure 7 shows that the effect of calibration drift can be much more important than the effects due to typical wire misalignment.

4. Turbulence results

Because the direction of the mean flow is continually varying with distance from the wall in a three-dimensional flow, it is not useful to represent the velocity fluctuations in a fixed coordinate system. Here, we define u' , v' and w' as the velocity fluctuations

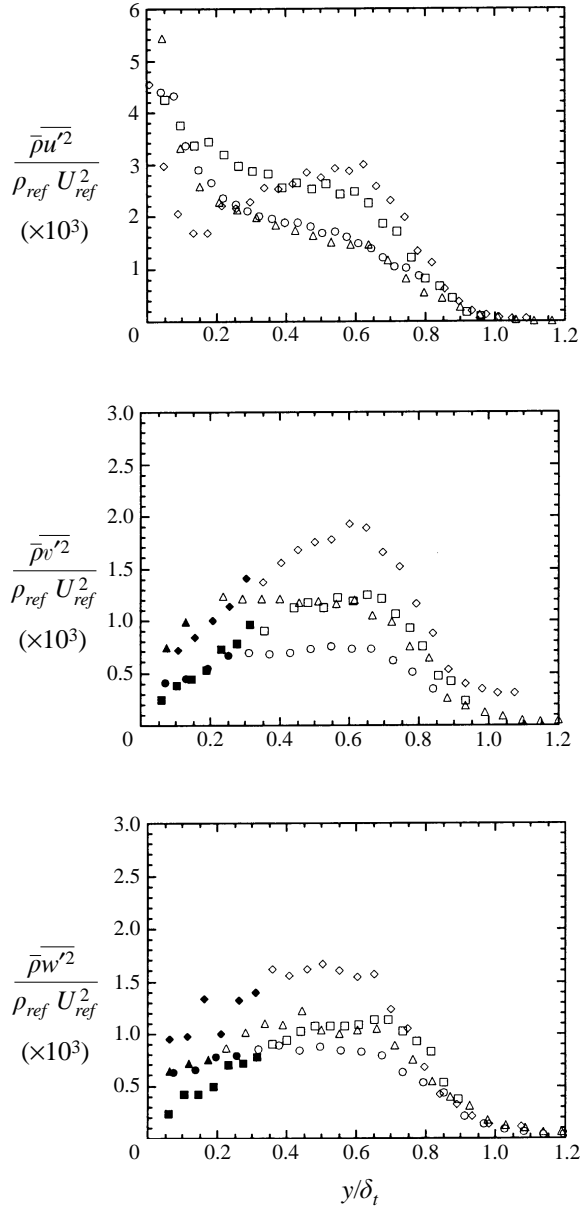


FIGURE 12. Normal Reynolds stresses normalized by the reference free-stream velocity and density. Symbols as in figure 11.

relative to the local mean flow direction, where u' is measured in the direction of the local mean velocity, v' is measured normal to the wall, and w' is in the mutually orthogonal direction.

The distribution of $\overline{u'^2}$, $\overline{v'^2}$ and $\overline{w'^2}$, non-dimensionalized by the free-stream velocity in the incoming boundary layer, are shown in figure 10. The level of $\overline{u'^2}$ is almost unchanged in the outer part of the layer, but $\overline{v'^2}$ and $\overline{w'^2}$ display a strong attenuation initially, especially in the region $0 < y/\delta_t < 0.5$, before relaxing slowly toward the upstream, undisturbed values. A decrease in the u' components is not seen until the downstream convergence region, where a steep drop occurs in the region near the wall,

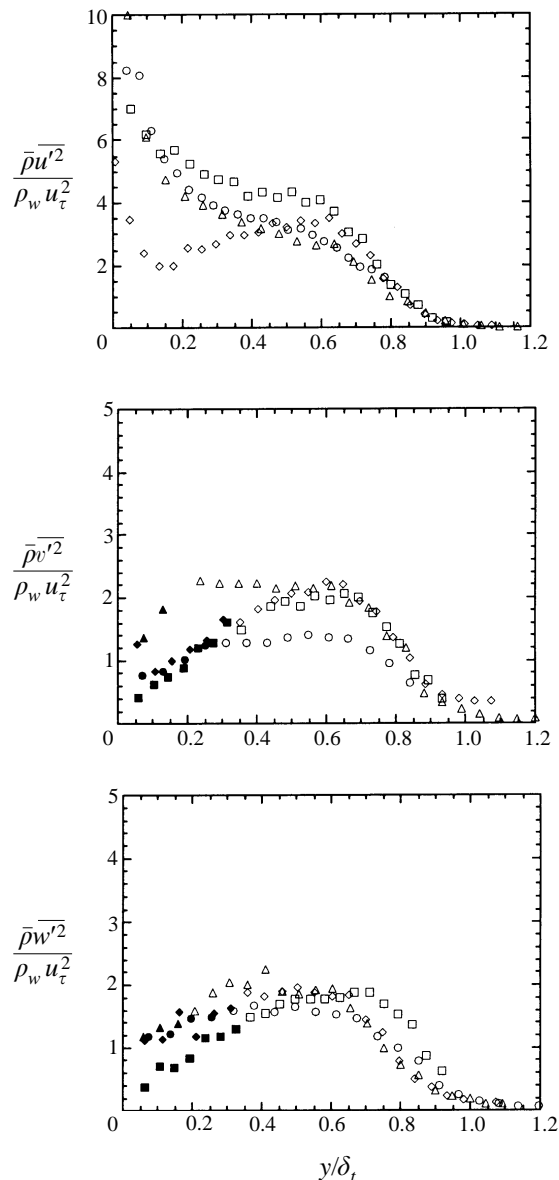


FIGURE 13. Normal Reynolds stresses normalized by the local wall stress. Symbols as in figure 11.

again related to the influx of high-momentum, low-turbulence fluid from the outer parts of the upstream boundary layer.

In subsonic studies, $\overline{w'^2}$ is always larger than $\overline{v'^2}$, even in distorted three-dimensional boundary layers. Ausherman & Yanta (1984) found the same result in a supersonic three-dimensional flow, where $\overline{w'^2}$ was larger than $\overline{v'^2}$ by about 50%. The results given in figure 10 indicate that the levels of $\overline{w'^2}$ and $\overline{v'^2}$ are nearly equal throughout. It is not clear why this is so, but Dussauge *et al.* (1995) noted that $\overline{v'^2}$ levels increase significantly with Reynolds number, and $\overline{v'^2}/\overline{w'^2}$ can exceed 1 at high Reynolds number. Hence the high levels of $\overline{v'^2}$ seen here could simply be due to the fact that the Reynolds number is very much higher than in most previous subsonic and supersonic experiments.

In figures 11–13, the turbulence intensities and the normal Reynolds stresses are

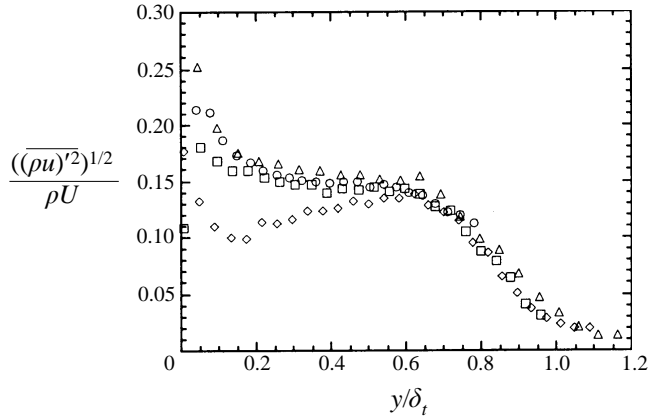


FIGURE 14. Streamwise mass flux normalized by the local velocity and density. Symbols as in figure 11.

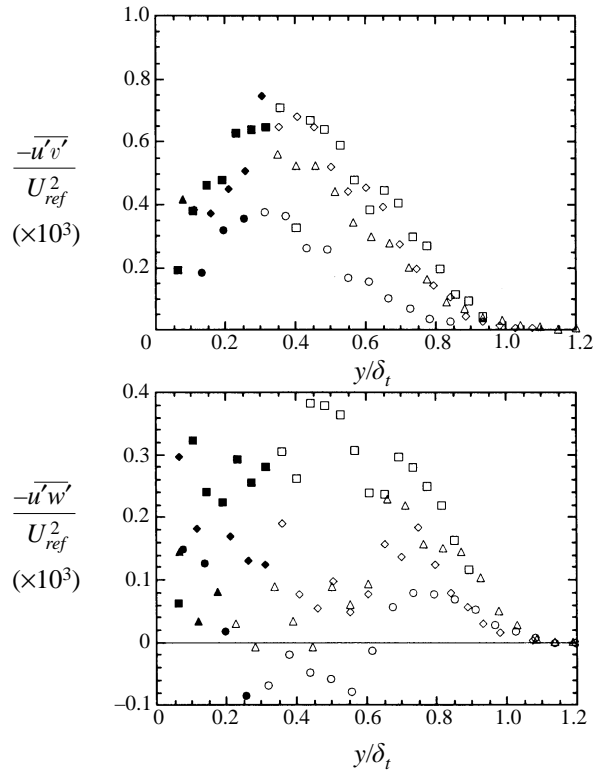


FIGURE 15. Kinematic Reynolds shear stresses normalized by the reference free-stream velocity. Symbols as in figure 11.

plotted using three different normalizations to explore possible similarity behaviour. No firm conclusions can be drawn. Since the quantities based on $\overline{v'^2}$ and $\overline{w'^2}$ behave very similarly, their scaling behaviour is also very similar. The marginally better collapse for the data non-dimensionalized using the local wall shear stress must be fortuitous since it is difficult to imagine that the local shear stress is an important parameter for a three-dimensional boundary layer outside the near-wall region. As for

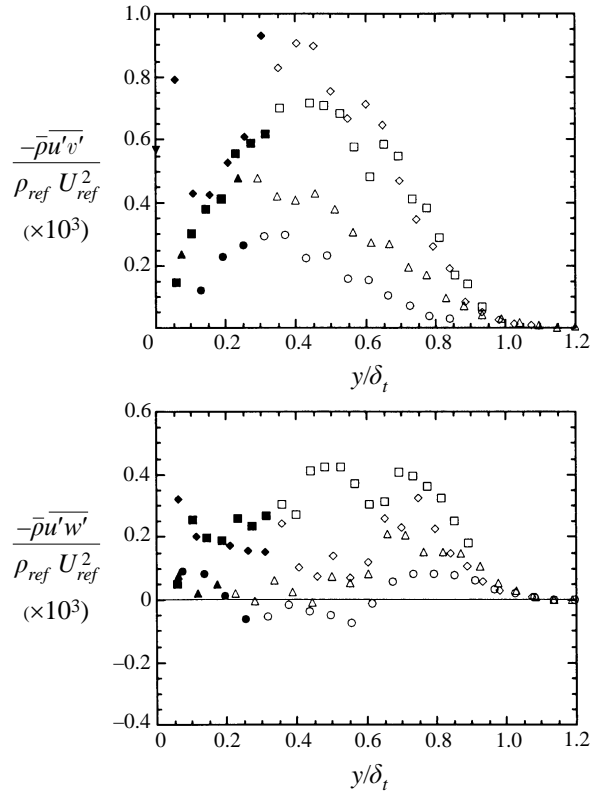


FIGURE 16. Reynolds shear stress normalized by the reference free-stream velocity and density. \blacktriangledown , $C_{f,ref}/2$. Other symbols as in figure 11.

the quantities based on the streamwise component, the upstream reference velocity is the most effective scaling parameter, indicating that the absolute levels of $\overline{u'^2}$ are conserved, at least in the outer region. To some extent this is true for the other quantities also, except for a rather rapid decrease associated with the first application of the adverse pressure gradients.

To complement this discussion, the streamwise mass flux fluctuations normalized by the local mean mass flow are given in figure 14. The trends in all the figures follow that shown by the kinematic normal stresses given in figure 11, again with the steep drop of the turbulence intensity at the furthest downstream location. Note that the mean free-stream mass flux increased by as much as 58% at the last location, that is, the mass flux fluctuations increased significantly, but $(\rho u)' / \bar{\rho} \bar{u} = \rho' / \bar{\rho} + u' / \bar{u}$, and a comparison of figures 11 and 14 shows that this behaviour is due almost exclusively to the increase in the magnitude of the density fluctuations.

The Reynolds shear stresses $-\overline{\rho u'v'}$ and $-\overline{\rho u'w'}$ are given in figures 15–17. The trends are well-represented by any one of the three non-dimensionalizations shown since the results do not show any particular similarity behaviour. For example, the kinematic shear stress $-\overline{u'v'}$ is increased at the two furthest downstream locations while the levels at the first downstream location show a drop in the stress levels (see figure 15). The other shear stress component $-\overline{\rho u'w'}$ is subject to greater error, but it can be seen that the levels increase downstream and that the highest levels for $-\overline{\rho u'w'}$ are at $X = 0.349$ m. Downstream of this station, the shear stress decreases slightly which is probably due to streamline curvature (see below for further discussion). The

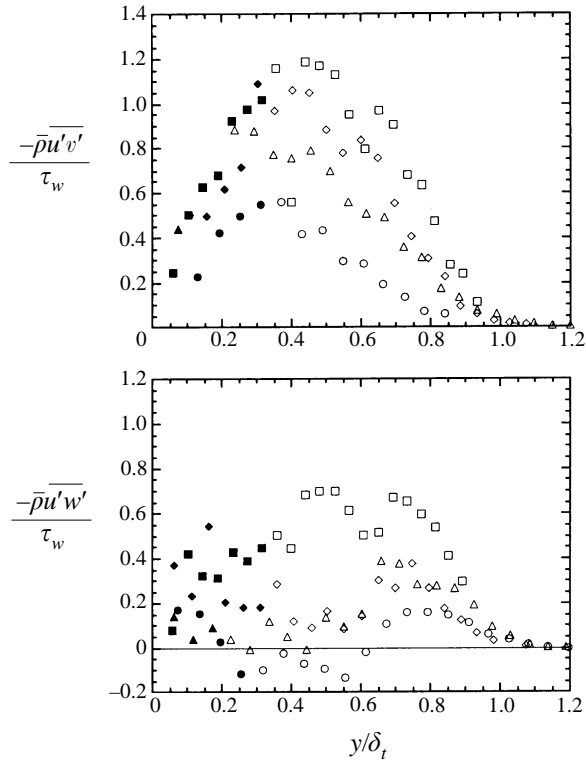


FIGURE 17. Reynolds shear stress normalized by the local wall stress. Symbols as in figure 11.

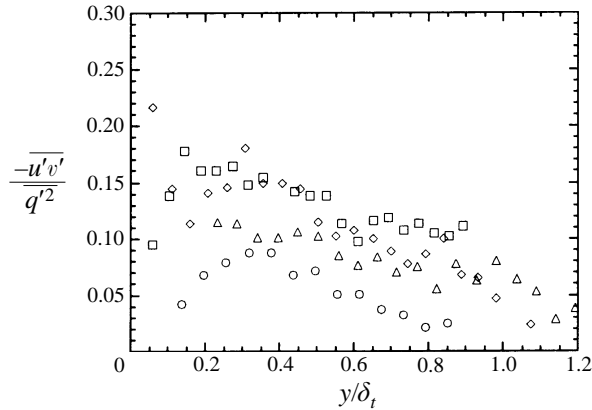


FIGURE 18. Townsend's structure parameter. Symbols as in figure 11.

highest values of $-\overline{\rho u'v'}$ are found at $X = 0.413$ m. The amplification in the outer part of the boundary layer at this location is linked directly to the pressure gradient history: the streamlines which pass through these points have experienced the strongest pressure gradients of all the points where turbulence data were obtained.

A number of other parameters are of interest, including the turbulence kinetic energy, anisotropy parameters, and the ratios of the normal stresses to the shear stresses. Here, in figure 18, we present only Townsend's parameter $a_1 = -\overline{u'v'}/q^2$, where $q^2 = \overline{u'^2} + \overline{v'^2} + \overline{w'^2}$ (the other quantities are given in Konrad 1993). The parameter a_1 was also measured by Fernando & Smits (1990) and the two sets of results agree very well

at the upstream location. Note, however, that here the measured value of q^2 was used as a normalizing parameter while Fernando & Smits adopted the approximation $\overline{q^2} = 1.5(\overline{u'^2} + \overline{v'^2})$, here given per unit mass. In both experiments the structure parameter decreases with distance from the wall and increases for increasing X , with the exception of the first measurement location downstream.

5. The effect of in-plane curvature

To evaluate the effects of streamline curvature (especially in-plane curvature) and pressure gradient history, it is useful to compare the current experiment to the study of a two-dimensional adverse pressure gradient by Fernando & Smits (1990) where the initial conditions were almost identical to those of the current investigation. In that case, the adverse pressure gradient was induced on the tunnel-floor boundary layer by compression waves emanating from a surface placed in the free stream.

The pressure gradient history for the three-dimensional curved-fin flow was determined using the computations reported by Konrad *et al.* (1994, 1998). For a given measurement station, the computational results were used to trace the origin of the mean streamline leading to each point in the profile. The pressure distributions along these streamlines were then determined from the computations, and the results were used to select mean streamlines that matched most closely the pressure history of the (two-dimensional) adverse pressure-gradient case. The comparisons between the computation and the experiment were generally very good in terms of the wall pressure, skin friction, and velocity profiles, so that we have some confidence in this procedure. The station that matched the pressure history well was located at $X = 0.413$ m. Naturally, different streamlines in the boundary layer experience somewhat different pressure histories, as can be seen in figure 19. However, if the pressure distributions were shifted somewhat in the coordinate s , measured along the streamline, the results nearly collapse onto a single curve, and all points in the profile experienced approximately the same pressure gradient history. (Note that the pressures across the boundary layer at the starting and ending points of the streamlines are approximately constant.)

To assess the effects of three-dimensionality and curvature, it is necessary to follow mean streamlines in each experiment since the mean streamlines do not start and end at the same height in the boundary layer. For example, in the three-dimensional case, high-momentum low-turbulence-intensity fluid in the incoming boundary layer is swept to positions close to the wall downstream. Consequently, fluid elements moving along mean streamlines that terminate at a given downstream location may start with a lower turbulence intensity. History effects are also important in the two-dimensional case because at this Mach number the pressure gradient decreases the boundary layer thickness. The streamline ending at a point in the downstream profile needs to be traced upstream so that the ratio of the upstream to the downstream turbulence intensity can be computed. The results of this analysis are shown in figure 20. The lower turbulence intensities found in the three-dimensional flow are consistent with the findings of many subsonic studies on the stabilizing influence of in-plane curvature. It was conjectured by Bradshaw & Pontikos (1985) that in-plane curvature tilts the eddies out of their preferred direction and therefore the Reynolds shear stress would be greatly reduced. Note that in the curved-fin flow the streamline at $y/\delta_t = 0.2$ exhibits quasi-in-plane curvature because it starts and ends at about the same height in the boundary layer. An inspection of the computed streamline coordinates (Konrad *et al.* 1994) shows that there is little curvature out of the plane parallel to the wall. As we can

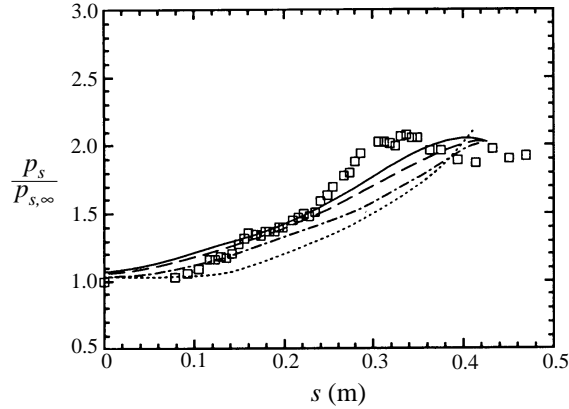


FIGURE 19. Static pressure distributions. \square , Wall pressure from Fernando & Smits (1990). Static pressures along streamlines for curved fin crossing the $Z = 0$ plane at $X = 0.413$ m and: —, $y/\delta = 0.02$; ---, $y/\delta = 0.06$; -·-, $y/\delta = 0.2$; ····, $y/\delta = 1.0$.

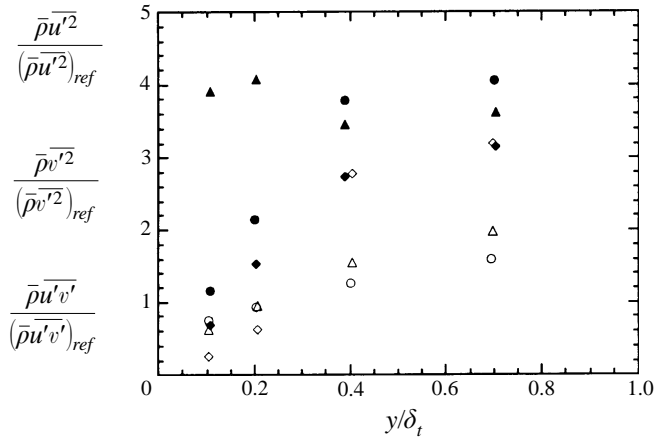


FIGURE 20. Relative turbulence amplifications: \blacktriangle , $\overline{u'^2}$; \bullet , $\overline{v'^2}$; \blacklozenge , $-\overline{u'v'}$ in Fernando & Smits's (1990) two-dimensional adverse-pressure-gradient flow; \triangle , $\overline{u'^2}$; \circ , $\overline{v'^2}$; \diamond , $-\overline{u'v'}$ in curved-fin flow at $X = 0.413$ m and $Z = 0$.

see from figure 20, for this particular streamline, the normal stresses throughout the layer are reduced very significantly below the level expected on the basis of the pressure-gradient history alone. Near the wall, all the shear stresses follow this trend, but in the outer layer the response seems to be virtually independent of the degree of in-plane curvature. This is somewhat surprising considering the strong effect on the normal stresses but it may reflect the lower level of in-plane curvature seen by the outer streamlines.

6. Summary and closing remarks

In the small-crossflow region, defined by a crossflow of less than 10° , the turbulence intensities and Reynolds shear stresses were found to decrease below their undisturbed levels. In the upstream convergence region, there was an increasing deflection of the velocity profile including the appearance of an inflection point, and a strongly increasing crossflow component up to 20° produced streamline curvature which is in-plane for the most part. Some similarity to two-dimensional adverse-pressure-gradient

flows was observed in the retardation of the mean velocity profiles. Turbulence levels were increased compared to the incoming boundary layer, due to the combined effects of pressure gradients from those of streamline curvature.

The downstream convergence region was dominated by strong three-dimensional effects, and the velocity profiles were accelerated strongly to levels beyond those in the upstream boundary layer due to diversion of high-momentum fluid from locations higher in the upstream boundary layer to locations closer to the wall. Streamline curvature in this region was more complex than in the upstream convergence region. In the downstream convergence region, the turbulence was compared to Fernando & Smits's (1990) equivalent adverse-pressure-gradient case and decreased turbulence intensities were found for all of the boundary layer profile. For one streamline, the effect of in-plane curvature could be approximately investigated and it was shown that the added effect of in-plane curvature decreased all Reynolds stresses with the largest decrease observed in the streamwise normal Reynolds stress.

The turbulence behaviour in the curved-fin flow may also be compared to the observation made by Tan in a 10° sharp-fin flow, where the turbulence intensities increase in the outer part of the boundary layer (see figure 2). Tan used the boundary layer thickness determined from the mean flow data rather than a 'turbulent' boundary layer thickness, so that it is difficult to tell directly from figure 2 how large the relative amplification is. Most importantly, the turbulence intensities in the downstream part in the interaction show the same trend as seen in the downstream part of the curved-fin flow. That is, the streamwise turbulence intensities first decrease near the wall and then rise again in a thin layer near the wall. The common feature is that high-momentum fluid, that is, low-turbulence-intensity fluid from the outer layer replaces the swept-away low-momentum fluid near the wall in both flows. Turbulence production near the wall is large enough to lead to an increase in turbulence intensities very close to the wall as part of the recovery process. The local minimum in the turbulence intensity profile, however, is more pronounced in the sharp fin-flow.

The work was sponsored by the Air Force Office of Scientific Research under AFOSR Grants 89-0033, 86-0266, F19620-93-0064, F49620-93-1-0427, F49620-93-1-0476, and F49620-93-1-0478.

REFERENCES

- ABELL, C. J. 1974 Scaling laws for pipe flow turbulence. PhD thesis, University of Melbourne.
- ALLEN, J. M. 1977 Reevaluation of compressible flow Preston tube calibrations. *NASA Tech. Mem. X-3488*.
- ALVI, F. S. & SETTLES, G. S. 1990 Structure of swept shock/wave boundary layer interactions using conical shadowgraphy. *AIAA Paper 90-1644*.
- AUSHERMAN, D. W. & YANTA, W. J. 1984 Mach 3 three-dimensional boundary layer turbulence transport properties on a spherically blunt cone. AFWAL Viscous and Interacting Flow Field Effects. In *Proc. 9th US Air Force and Federal Republic of Germany Data Exchange Agreement Meeting*, pp. 155-178.
- BERG, B. VAN DEN 1975 A three-dimensional law of the wall for turbulent shear flows. *J. Fluid Mech.* **70**, 149-160.
- BRADSHAW, P. 1973 Effects of streamline curvature on turbulent flow. *AGARDograph* 169.
- BRADSHAW, P. & PONTIKOS, A. S. 1985 Measurements in the turbulent boundary layer on an 'infinite' swept wing. *J. Fluid Mech.* **159**, 105-130.
- BRADSHAW, P. & UNSWORTH, K. 1974 Comment on 'evaluation of Preston tube calibration equations in supersonic flow'. *AIAA J.* **12**, 1293-1295.
- BRAUN, W. H. 1958 Turbulent boundary layer on a yawed cone. *NACA Tech. Note* 4208.

- BROWN, J. D., BROWN, J. L. & KUSSOY, M. I. 1988 A documentation of two- and three-dimensional shock-separated turbulent boundary layers. *NASA Tech. Mem.* 101008.
- CLAUSER, F. H. 1956 The turbulent boundary layer. *Adv. Appl. Mech.* **4**, 1–51.
- COOKE, J. C. 1958 A calculation method for three-dimensional turbulent boundary layers. *Aeronaut. Res. Council R. & M.* 3199.
- DEGANI, A. T. 1991 The three-dimensional turbulent boundary-layer – theory and application. PhD thesis, Mechanical Engineering Department, Lehigh University.
- DELEUZE, J. & ELÉNA, M. 1995 Quelques caractéristiques de la turbulence en aval d’une inter-action onde de choc couche limite. *12ème Congrès Français de Mécanique, Strasbourg, France.*
- DEMETRIADES, A. & McCULLOUGH, G. 1985 Mean-flow measurements in a supersonic three-dimensional turbulent boundary layer. *J. Fluid Mech.* **156**, 401–418.
- DONOVAN, J. F. & SPINA, E. F. 1992 An improved analysis method for cross-wire signals obtained in supersonic flow. *Expts. Fluids* **12**, 359–368.
- DRIEST, E. R. VAN 1951 Turbulent boundary layer in compressible fluids. *J. Aeronaut. Sci.* **18**, 145–160, 216.
- DUSSAUGE, J. P., FERNHOLZ, H., FINLEY, P. J., SMITH, R. W., SMITS, A. J. & SPINA, E. F. 1995 Turbulent boundary layers in subsonic and supersonic flow. *AGARDograph* 335.
- FERNANDO, E. M. & SMITS, A. J. 1990 Supersonic turbulent boundary layer in an adverse pressure gradient. *J. Fluid Mech.* **221**, 285–307.
- GAVIGLIO, J., ANGUILLET, J.-P. & ELENA, M. 1981 On the application of hot-wire anemometry to the solution of problems arising in variable temperature turbulent flows. *Rech. Aérop.* **1**, 59.
- HALL, M. G. 1965 Experimental measurements in a three-dimensional turbulent boundary layer in supersonic flow. *AGARDograph* **97**, Part 2, pp. 829–853.
- JOHNSON, D. A. & ROSE, W. C. 1975 Laser velocimeter and hot-wire anemometer comparison in a supersonic boundary layer. *AIAA J.* **13**, 512–515.
- JOHNSTON, J. P. 1960 On the three-dimensional turbulent boundary layer generated by secondary flow. *Trans. ASME D: J. Basic Engng.* **82**, 233–248.
- KIM, K.-S., LEE, Y. & SETTLES, G. S. 1991 Laser interferometer/Preston tube skin-friction comparison in shock/boundary-layer interaction. *AIAA J.* **29**, 1007–1009.
- KISTLER, A. L. 1959 Fluctuation measurements in a supersonic turbulent boundary layer. *Phys. Fluids* **2**, 290–296.
- KNIGHT, D., HORSTMAN, C., SHAPEY, B. & BOGDONOFF, S. 1986 The flowfield structure of the 3-D shock wave/boundary-layer interaction generated by a 20 deg sharp fin at Mach 3. *AIAA Paper* 86-0343.
- KONRAD, W. 1993 A three-dimensional supersonic turbulent boundary layer generated by an isentropic compression. PhD thesis, Dept. of Mechanical & Aerospace Engineering, Princeton University.
- KONRAD, W. & SMITS, A. J. 1993 Reynolds stress measurements in a three-dimensional supersonic turbulent boundary layer. *Proc. Third Intl Symp. on Thermal Anemometry*. In (ed. D. E. Stock, A. J. Smits, S. A. Sheriff & J. Davidson). ASME FED, Vol. 132.
- KONRAD, W., SMITS, A. J. & KNIGHT, D. 1994 A combined experimental and numerical study of a three-dimensional supersonic turbulent boundary layer. *Expl Thermal Fluid Sci.* **9**, 156–164.
- KONRAD, W., SMITS, A. J. & KNIGHT, D. 1998 Mean flow field structure of a three-dimensional supersonic turbulent boundary layer. *AIAA J.* To appear.
- KUSSOY, M. I., BROWN, J. D., BROWN, J. L., LOCKMAN, W. K. & HORSTMAN, C. C. 1987 Fluctuations and massive separation in three-dimensional shock-wave/boundary-layer interactions. *Second Intl Symp. on Transport Phenomena in Turbulent Flows*, pp. 875–887.
- MAGER, A. 1952 Generalization of boundary-layer momentum-integral equations to three-dimensional flows including those of rotating system. *NACA Rep.* 1067.
- PANARAS, A. G. 1992 Numerical investigation of the high-speed conical flow past a sharp fin. *J. Fluid Mech.* **236**, 607–633.
- PERRY, A. E. & JOUBERT, P. N. 1965 A three-dimensional turbulent boundary layer. *J. Fluid Mech.* **22**, 285–304.
- PERRY, A. E., LIM, K. L., HENBEST, S. M. & CHONG, M. S. 1983 Rough- and smooth-walled shear flows. *Proc. 4th Intl Symp. on Turbulent Shear Flow*, Karlsruhe, Germany.

- SETTLES, G. S. 1975 An experimental study of compressible turbulent boundary layer separation at high Reynolds numbers. PhD thesis, Aerospace and Mechanical Sciences Department, Princeton University.
- SETTLES, G. S. & TENG, H.-Y. 1983 Flow visualization methods for separated three-dimensional shock wave/boundary layer interactions. *AIAA J.* **21**, 390–397.
- SHAPEY, B. & BOGDONOFF, S. M. 1987 Three-dimensional shock wave/turbulent boundary layer interaction for a 20 deg sharp fin. *AIAA Paper* 87-0554.
- SMITH, D. R., FERNANDO, E. M., DONOVAN, J. F. & SMITS, A. J. 1992 Conventional skin friction measurement techniques for strongly perturbed supersonic boundary layers. *Eur. J. Mech. B/Fluids* **11**, 719–740.
- SMITS, A. J., HAYAKAWA, K. & MUCK, K. C. 1983 Constant temperature hot-wire anemometry practice in supersonic flow, Part I: The normal wire. *Expts. Fluids* **1**, 83–92.
- SMITS, A. J. & MUCK, K. C. 1984 Constant temperature hot-wire anemometry practice in supersonic flow, Part II: The inclined wire. *Expts. Fluids* **2**, 33–41.
- SPINA, E. F., SMITS, A. J. & ROBINSON, S. K. 1994 The physics of supersonic turbulent boundary layers. *Ann. Rev. Fluid Mech.* **26**, 287–319.
- TRANS, T. T., TAN, D. K. M. & BOGDONOFF, S. M. 1985 Surface pressure fluctuations in a three-dimensional shock wave/turbulent boundary layer interaction at various shock strengths. *AIAA Paper* 85-1562.
- YANTA, W. J., AUSERMAN, D. W. & HEDLUND, E. 1982 Measurements of a three-dimensional boundary layer on a sharp cone at Mach 3. *AIAA Paper* 82-0289.